Structure and magnetic properties of ferromagnetic nanowires in self-assembled arrays

H. Zeng,[1,3,*] R. Skomski,[1,3] L. Menon,[2,3] Y. Liu,[3,4] S. Bandyopadhyay,[2,3] and D. J. Sellmyer[1,3]
[1]*Department of Physics and Astronomy, University of Nebraska, Lincoln, Nebraska 68588*
[2]*Department of Electrical Engineering, University of Nebraska, Lincoln, Nebraska 68588*
[3]*Center for Materials Research and Analysis, University of Nebraska, Lincoln, Nebraska 68588*
[4]*Department of Mechanical Engineering, University of Michigan, Ann Arbor, Michigan 48109*
(Received 13 October 2000; revised manuscript received 1 June 2001; published 20 March 2002)

Static and dynamic aspects of the magnetization reversal in nanowire arrays are investigated. The arrays have been produced by electrodeposition of ferromagnetic metals (Fe, Co, and Ni) into porous anodic alumina templates, with diameters as small as 5 nm. The crystal structures of the nanowires are bcc (Fe) and fcc (Ni) and a mixture of fcc and hcp (Co), with grain sizes of a few nanometers. Magnetic properties as a function of temperature are investigated. The temperature dependence of coercivity can be understood in terms of thermal activation over an energy barrier with a $\frac{3}{2}$-power dependence on the field. Coercivity as a function of diameter reveals a change of the magnetization reversal mechanism from localized quasicoherent nucleation for small diameters to a localized curlinglike nucleation as the diameter exceeds a critical value determined by the exchange length. The quasicoherent limit is described by a model that yields explicitly real-structure-dependent expressions for coercivity, localization length, and activation volume.

DOI: 10.1103/PhysRevB.65.134426 PACS number(s): 75.30.Gw, 75.60.Ej, 75.70.Cn

I. INTRODUCTION

Fundamental interest in ferromagnetic nanowire and nanoparticle arrays lies in the emergence of novel magnetic and transport properties as the dimension approaches the length scale of a few nanometers to a few tens of nanometers. For example, conductance and flux quantization have been observed for ferromagnetic nanowire arrays[1,2] and giant magnetoresistence is realized in multilayer-structured nanowires.[3] Current interest in research on ferromagnetic nanowires is stimulated by the potential application to future ultra-high-density magnetic recording media[4,5] and electronic devices.[6] Commonly used methods to produce nanoarrays involve lithographic patterning,[7] which is an extremely slow and costly process. Recently, self-assembly has been suggested as a promising technique for preparing ordered nanoarrays because of its low cost, high yield, and the ability to achieve extremely small features.[4]

The magnetic nanowire arrays investigated in this work are produced by electrodeposition into self-assembled alumina pores. When aluminum is anodized in an acid electrolyte, aluminum oxide with self-assembled nanosized densely packed pore arrays will form. The diameter, center-to-center spacing between the pores and lengths of the pores can be easily controlled by varying the electrochemical parameters. Highly ordered arrays can be produced utilizing special electrochemical techniques.[8] Magnetic materials such as Fe, Co, and Ni can be grown by electrodeposition as nanowires in such templates. Studies on magnetic properties of such systems and their potential application to recording media date back to the 1970s and 1980s.[9] The nanowires exhibit uniaxial anisotropy, with their easy axes aligned along the wire axes and perpendicular to the film plane. The strong perpendicular anisotropy has been attributed to magnetic shape anisotropy.[10]

As indicated in a recent review by Sellmyer, Zheng, and Skomski,[11] the physical phenomena and potential applications require a deep understanding of the magnetism of nanowires. A key problem in the magnetism of nanowires is understanding the magnetic reversal mechanism. Since magnetization reversal is hysteretic, it involves metastable energy barriers. This leads to two key problems: how an applied magnetic field yields a static magnetization reversal and how thermally activated jumps over energy barriers modify the hysteresis (dynamic reversal). In perfect ellipsoids of revolution subject to a field parallel to the long axis, magnetization reversal starts by coherent rotation or curling, although there remains a remote possibility of a buckling mode.[12] The transition between the two modes depends on the radius of the ellipsoid. For infinite cylinders, coherent rotation occurs when the diameter is smaller than $2.08A^{1/2}/M_s$ and curling in thicker wires. Dynamic reversal involves jumps over energy barriers. Since coherent rotation and curling modes are delocalized,[12] the corresponding activation volume scales as the particle volume and diverges for long wires. In fact, experimental evidence speaks in favor of coherent rotation[13] and curling[14] in nanoscale particles with relatively small aspect ratios, but neither observed coercivities nor activation volumes support delocalized reversal for elongated nanowires (see Ref. 15, and references therein). The reason for this is that deviations from the limit of perfect ellipsoids of revolution give rise to localized nucleation.[15] However, to our best knowledge, no explicit energy barrier calculations have been made to treat static and dynamic reversal effects on a common footing and to derive them from real-structure models.

In this work, we investigate magnetic properties between room temperature and liquid-helium temperature for varying nanowire diameters. To explain the observed static and dynamic properties of thin wires, a magnetization reversal model is developed, solved, and used to explain the experimental data. The behavior of thinner wires is ascribed to quasicoherent and thicker wires' curlinglike mechanisms, both realized in a localized region.

II. EXPERIMENT

The starting template material, 99.99% pure Al foil, was electropolished in a standard L1 electrolyte. The foil was then dc anodized in acidic solutions to form a layer of porous alumina. ac electrodeposition was used due to the dielectric nature of alumina.[16] For deposition of Co, an electrolyte containing 0.1 M $CoSO_4$ was used, either with or without boric acid; for deposition of Fe and Ni, $CoSO_4$ was substituted by $FeSO_4$ and $NiSO_4$, respectively. The center-to-center spacing (D) and the diameter of the nanowires (d_w) can be readily controlled by electrochemical parameters. Through the use of different electrolytes and with varying voltages, nanowires with diameters ranging from 5 to 40 nm have been produced.

The structure of the deposited material was characterized by transmission electron microscopy (TEM), high-resolution TEM, selected-area diffraction, and nanodiffraction. Nanowires were released from the template, and were picked up by a copper grid coated with carbon films for TEM observations. Approximately 20 wires were measured to obtain the mean diameter d_w and diameter distributions. The magnetic properties of nanowires embedded in the anodic alumina template were measured by an alternating-gradient-force magnetometer and a superconducting quantum-interference-device magnetometer.

III. RESULTS

A. Structural properties

The anodic alumina template contains self-assembled pore arrays with quasihexagonal ordering. The average center-to-center spacing (D) and pore diameter (d_p) depend on anodization conditions and the electrolyte used. For example, under an anodization voltage of 10 V at 20 °C, with 15% sulfuric acid, d_p is around 9 nm, D is about 35 nm, and the pore density exceeds 10^{11} cm^2. Our results show that both d_p and D are well defined, with variations of less than 5%. The length of the pores is typically several microns depending on the anodization time. The reader is referred to Ref. 16 for details.

The average wire diameter d_w is roughly equal to the average pore diameter. The variation in d_w, as observed from TEM images, is larger than that in d_p, most probably due to the fact that wire releasing is a potentially damaging process, and also some grains may be invisible due to their crystalline orientations. A rough estimate of the variation in wire thickness, based on TEM images, is about 20%. The wire length (L) depends on deposition time. In this study, L ranges from 1 to 5 μm to keep the aspect ratio (L/d_w) greater than 50.

All Fe, Co, and Ni nanowires are polycrystalline. Figure 1 shows some typical TEM images and selected-area-diffraction patterns of Fe, Co, and Ni nanowires freed from the anodic alumina template. Figures 1(a) and 1(b) are image and diffraction patterns of the bcc Fe nanowire sample. The crystallite size is so small that it is not discernable in the image, and the corresponding diffraction ring is very broad compared to that of Co and Ni wires. However, at the opposite extreme, Fe nanowires having crystallite sizes of about 40 nm along the wire axis have also been produced. For comparison, Ni nanowires consist of fcc crystallites characterized by sizes of about 10 nm, as seen in Figs. 1(e) and 1(f). The nanostructure of Co wires is more complicated. Crystallite size can be as large as a few tens of nanometers, and a single wire consists of a chain of single crystallites; or the crystallites can be extremely small, about 2–3 nm, and the cross section of a wire consists of 5–10 grains. The Co nanowires consist either of mostly hcp or fcc grains or a mixture of both. While fcc is a metastable phase for bulk Co, it is typically seen in Co nanoparticles or ultrathin films. Figure 1(d) shows the diffraction ring pattern of fcc and hcp mixtures of a typical Co nanowire sample. For samples that contain mostly the hcp phase, we observe no preferential orientation of the Co c axis, and the crystalline size is extremely small (about 2–3 nm).[16] The size of the crystallites of Fe, Co, and Ni nanowires, as well as the crystalline structure of the Co nanowires, depend on deposition conditions such as the ac frequency, pH value of the solutions, and the chemical treatment of the as-anodized template before deposition, which will be discussed elsewhere.

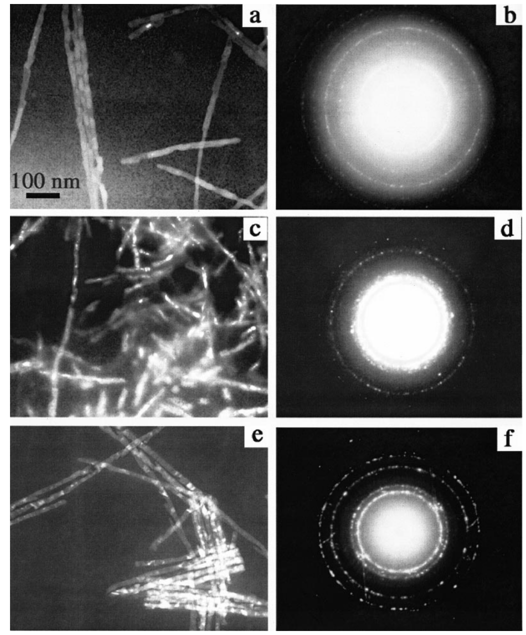

FIG. 1. Selected reflection images and TEM diffraction patterns of (a) and (b) Fe, (c) and (d) Co, and (e) and (f) Ni nanowires.

B. Anisotropy

Typically, nanowire arrays possess uniaxial anisotropy, with the easy axis aligned along the wire axis and perpendicular to the plane. It is well known that the main origin of the magnetic anisotropy is shape anisotropy. Hysteresis loops measured perpendicular to the film plane show remanence ratios ($S=M_r/M_s$) greater than 0.9. Theoretically, the shape anisotropy field (H_K) for an infinite cylinder is $2\pi M_s$, where M_s is the saturation magnetization. M_s at room temperature is 1707, 1400, and 485 emu/cm^3 for bulk Fe, Co, and Ni, respectively. The corresponding H_K values calculated are 11 000, 8800, and 3400 Oe, respectively. The effective perpendicular anisotropy fields measured by extrapolating magnetization curves are 10 000, 7500, and 3000 Oe, respectively, which are smaller than but fairly close to the theoretical limits. These values are roughly independent of nanowire diameter, at least for thin wires ($d_w < 15$ nm). Likely contributions to the small discrepancies are wire inhomogeneities and a reduction of the saturation magnetization in nanowires, as compared to bulk materials.

Secondary anisotropy contributions are bulk and surface magnetocrystalline anisotropy, magnetoelastic anisotropy due to stress, and anisotropy associated with morphological imperfections, such as wire-diameter fluctuations and wire ends. Although the measured anisotropy is close to the theoretical values, it will be shown later that these factors may lead to the reduction of the energy barrier and the coercivity during magnetization reversal. The reason that magnetocrystalline anisotropy of Co does not strongly affect the total anisotropy of the wire is probably due to the extremely small grain size together with random orientations, so that local anisotropy tends to average out.[17] The existence of a significant amount of the fcc phase and stacking faults also lowers the magnetocrystalline anisotropy. There might also be some magnetoelastic anisotropy, but for the present samples the stress is very low due to our preparation conditions, and no stress effect on anisotropy and coercivity has been observed.

C. Room-temperature coercivity

Our previous work[16] on Co nanowire arrays showed that the room-temperature coercivity depends strongly on the wire length. It was found that for constant diameter d_w and spacing D, the coercivity (H_c) initially increases rapidly as a function of wire length, and then approaches saturation when L/d_w exceeds 5. A similar length dependence of H_c is also obtained for Fe and Ni wires. The saturated H_c values are generally three to four times smaller than the anisotropy field values.

H_c as a function of d_w for Fe, Co, and Ni nanowires with constant D is shown in Fig. 2. A key problem in the understanding of the magnetism of nanowires is the diameter dependence of the coercivity.[12] For Co, H_c decreases monotonically with increasing d_w except for the smallest d_w; for Fe and Ni nanowires, H_c as a function of d_w shows a maximum. It is difficult to explain the decrease of H_c with decreasing diameter without taking into account thermal fluctuations. The influence of thermal fluctuations is also supported by the magnetic viscosity and temperature dependence of coercivity behavior (Secs. III D and III E). Several possibilities could account for the decrease of H_c with increasing d_w. In the case of curling, H_c changes linearly with $1/d_w^2$,[12] and the predicted diameter for the transition from coherent rotation to curling is within the range of this study. In Secs. III E and III F we will see that the reversal mechanism is more complicated. Accompanying the decrease of H_c with increasing d_w, the hysteresis loops also become more and more skewed, and the remanence value decreases as well, which indicates increasing magnetostatic interactions as wires get closer together.[16]

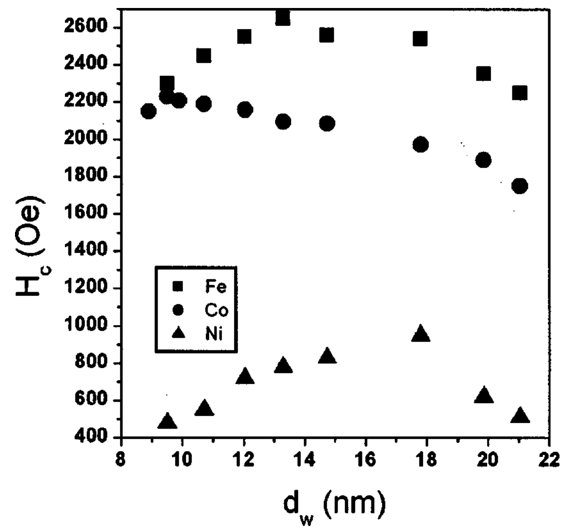

FIG. 2. H_c as a function of nanowire diameter d_w for Fe, Co, and Ni, respectively.

D. Magnetic viscosity and activation volume

It has been known for several years that like any small magnetic particles, magnetic nanowires show strong magnetic-viscosity effects[18] as well as a field-sweep-rate dependence of coercivity,[13] suggesting that thermal fluctuations play a vital role in nanowire magnetism. An effective volume that is involved in the thermally activated magnetization reversal process is called the thermal activation volume (V^*). The interpretation of V^* is generally complicated, though in the case of a single energy barrier, V^* can be defined as

$$V^* = -\frac{1}{M_s}\frac{\partial E_B(H)}{\partial H}. \tag{1}$$

V^* measurements can be used to assist in understanding the magnetization reversal process and energy barrier that is responsible for magnetization reversal.

For this purpose, V^* for Fe, Co, and Ni nanowires with varying d_w has been measured by the waiting-time method, which involves magnetization decay measurements.[19,20] The activation volume V^* is given by

$$V^* = \frac{k_B T}{M_s \cdot \left.\left(\dfrac{H_2 - H_1}{\ln t_2 - \ln t_1}\right)\right|_{M_{\mathrm{irr}}}}, \tag{2}$$

where t_1 (t_2) is the waiting time for the saturation magnetization to decay to the magnetization value M at an applied field H_1 (H_2). Equation (2) is suitable for systems with perpendicular anisotropy.[19]

Contrary to previous reported results that $V^* \approx \frac{1}{20}V$,[20] we found that V^* as a function of wire length approaches a constant value for a large aspect ratio (>50).[16] We have compared V^* of wires with crystallite sizes mostly of 2–3 nm with those consisting of mostly single crystallites of several tens of nanometers, other conditions identical. We found that V^* remains nearly unchanged. On the other hand, V^* is strongly dependent on diameter. V^* for Fe, Co, and Ni

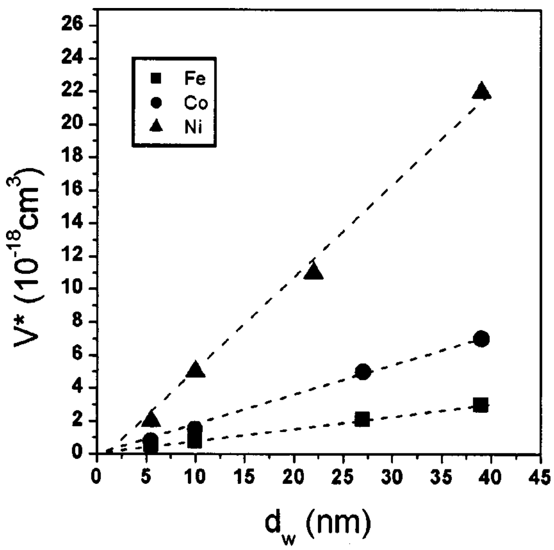

FIG. 3. V^* as a function of d_w for Fe, Co, and Ni nanowires, respectively. The dashed lines are guides to the eye.

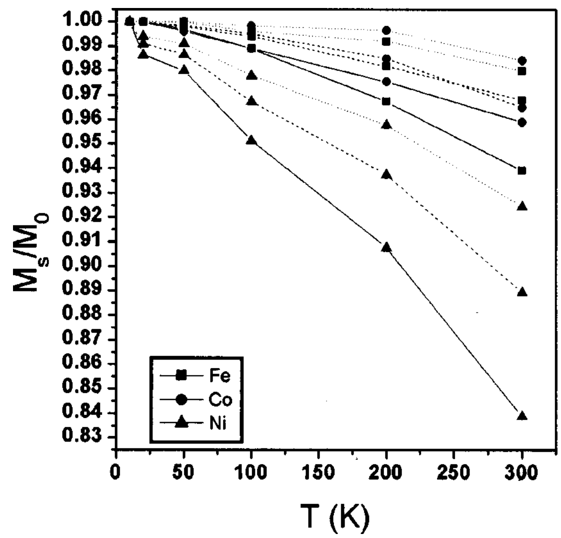

FIG. 4. Normalized saturation magnetization M_s as a function of temperature for Fe, Co, and Ni nanowires. d_w=5.5 nm (solid lines), 10 nm (dashed lines), and 27 nm (dotted lines).

nanowires as a function of d_w is plotted in Fig. 3. At identical diameters, V^* of Fe is the smallest and that of Ni is the largest. The seemingly linear diameter dependence of V^* is probably accidental, which may reflect the crossover of reversal mechanisms as well as the change in anisotropy with changing diameter. Therefore, one may conclude that V^* is both dimension and material dependent. It is also probable that local structural and compositional inhomogeneities may affect V^* and complicate the structural dependence.

Room-temperature measurements show the following facts. H_c of nanowires is much smaller than predicted for coherent rotation or curling. Also, there are strong magnetic-viscosity effects, and activation volumes are a hundred times smaller than wire volumes. These indicate that magnetization reversal cannot be explained by simple reversal models. Several recent theoretical studies on the reversal of nanoscale magnets predict that for nanowires with a large aspect ratio, the reversal proceeds in a nucleation/propagation manner.[15,21–23] Several experimental studies reveal the relevance of the curling model, based on the measured angular dependence of the switching field; however, the fitted aspect ratio is much smaller than the actual value.[14,24]

The following sections (Secs. III E and III F) focus on the temperature-dependent magnetic properties. The purpose is to see whether thermal activation over an energy barrier picture is useful in describing finite-temperature coercivity for nanowire arrays, and to understand the physical origin of the reduction of energy barriers.

E. Temperature dependence of coercivity

Magnetic hysteresis loops were measured for samples with various diameters in the temperature range 10–300 K, from which M_s, H_K, and H_c as functions of temperature were determined. All samples have packing fractions ($P \approx d_w{}^2/D^2$) of about 0.05, so that interwire interactions can be neglected without introducing significant error.[16] Figure 4 shows the normalized M_s as a function of temperature for representative samples. Generally speaking, $M_s(T)$ of nanowires decreases faster than bulk materials. As the diameter d_w decreases, the change in M_s gets larger. This is to be expected, since as the wire gets thinner, surface effects become dominant. At identical d_w, M_s decreases the fastest for Ni and the slowest for Co, which is in accord with the Curie temperature of each material.

For all samples measured, the anisotropy field H_K is only a weak function of the temperature. H_K decreases only slightly as temperature increases from 10 to 300 K. The sample that shows the largest change in H_K with temperature is that of Ni nanowires with a 5.5-nm diameter. H_K decreases approximately 13% from 10 to 300 K, which can mainly be attributed to the temperature dependence of M_s. This confirms our suggestion that the main origin of anisotropy is shape anisotropy. If other effects such as magnetocrystalline anisotropy or stress contribute a significant portion of the total anisotropy, they are likely to cause the total anisotropy to show strong temperature dependence.

The temperature dependence of coercivity for nanowires has been reported by several groups.[25,26] In those studies, a linear relationship is assumed; however, not enough data is presented to confirm the linearity.

H_c as a function of temperature for typical Fe, Co, and Ni samples is shown in Fig. 5. H_c decreases with increasing temperature, the variation being more rapid at low temperatures. A detailed analysis shows that the temperature dependence of intrinsic properties, which determines the anisotropy field, could only account for a small portion of the H_c change. Therefore, the main characteristics of this temperature dependence must originate from thermal fluctuations. Thermal activation over a single energy barrier was proposed by Néel[27] and Brown.[28] The field dependence of the energy barrier has the form

$$E_B = E_0(1 - H/H_0)^m, \tag{3}$$

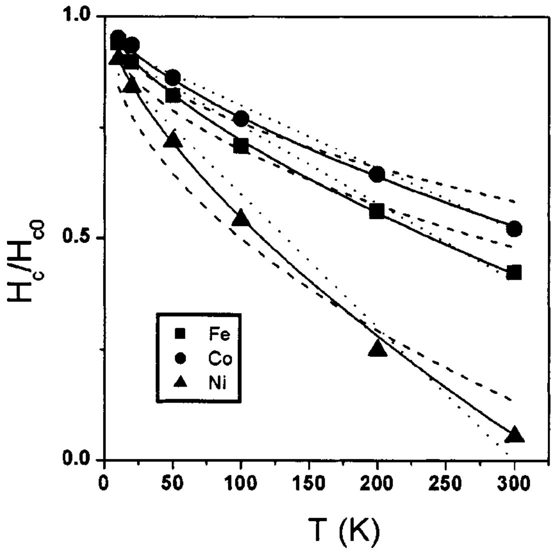

FIG. 5. H_c/H_{c0} as a function of temperature for Fe, Co, and Ni nanowires with $d_w = 5.5$ nm, where H_{c0} is the zero-temperature coercivity. The lines are fitting curves using Eq. (7) with $m = \frac{3}{2}$ (solid line), 2 (dashed line), and 1 (dotted line).

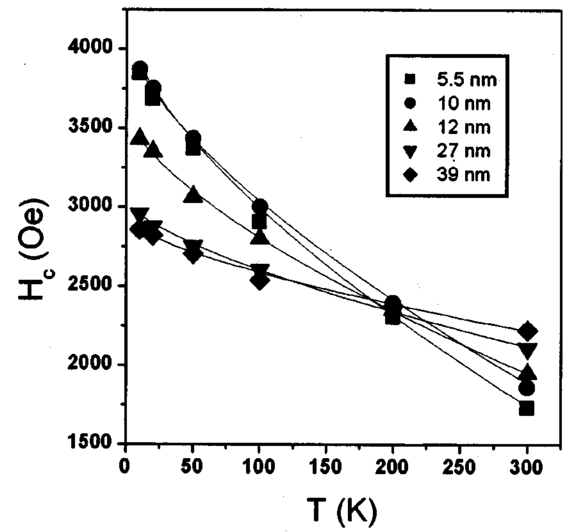

FIG. 6. Coercivity as a function of temperature for Fe nanowires with varying d_w.

where H_0 is the switching field without thermal fluctuation, and E_0 is barrier height with no field applied. For the special case of aligned Stoner-Wohlfarth particles, $m = 2$. It can be shown that m is in general equal to $\frac{3}{2}$, which is a natural result of a nonsymmetric energy landscape.[29] A linear field dependence of E_B is also sometimes employed but there is little theoretical justification for such behavior.

The relaxation time τ characterizing the process of the thermal activation of the magnetization over an energy barrier is given by

$$1/\tau = f_0 \exp(-E_B/k_B T), \tag{4}$$

where E_B is the energy barrier and f_0 is the attempt frequency typically of order 10^9 Hz. Assuming the typical measurement time to be 100 s, we then have

$$E_B = k_B T \ln f_0 \tau = 25 k_B T. \tag{5}$$

After a simple calculation from Eqs. (3) and (5), we obtain the coercivity due to thermal activation to be

$$H_c(T) = H_0(T)\{1 - [25 k_B T/E_0(T)]^{1/m}\}. \tag{6}$$

If the energy barrier is controlled by an effective shape anisotropy, H_0 is proportional to M_s and $E_0 \propto M_s{}^2$, that is, $H_0(T) = H_{c0} M_s(T)/M_{s0}$ and $E_0(T) = E_{00} M_s{}^2(T)/M_{s0}{}^2$, where H_{c0}, M_{s0}, and E_{00} represent quantities at zero temperature. Thus the temperature dependence of intrinsic properties can be taken into account explicitly. Equation (6) then becomes

$$H_c(T) = H_{c0} \frac{M_s(T)}{M_{s0}} \left[1 - \left(\frac{25 k_B T M_{s0}{}^2}{E_{00} M_s{}^2(T)} \right)^{1/m} \right]. \tag{7}$$

M_{s0} can be extrapolated from the $M_s(T)$ curve, and H_{c0}, E_{00}, and m are parameters to be determined from the fitting. If there are significant contributions from other effects such as magnetocrystalline anisotropy, Eq. (7) should not fit the experimental data.

In Fig. 5, the normalized coercivity (H_c/H_{c0}) as a function of T for Fe, Co, and Ni samples with $d_w = 5.5$ nm is shown, together with fits to Eq. (7) with $m = 2$, $\frac{3}{2}$, and 1, respectively. It is clearly seen that for all three samples, only the curves with $m = \frac{3}{2}$ match almost every data point. Neither $m = 2$ nor 1 can fit the whole temperature range as well as $m = \frac{3}{2}$, although it is noted that all of them probably can fit the data nearly equally as well for T from 100 to 300 K. Interestingly, a recent work also obtained $m = \frac{3}{2}$, although the temperature dependence of intrinsic properties was ignored.[30]

In the case of the diameters considered in Fig. 5, room-temperature coercivities of Co and Fe wires are about 45% and 55% smaller than the respective values at 10 K. By contrast, Ni at room temperature shows superparamagnetic behavior, with H_c close to zero; however, H_c increases dramatically to 1000 Oe with temperature decreased to 10 K. This indicates how important thermal fluctuations are in the magnetic behavior of nanowires. Comparing theoretical results with room-temperature data may therefore be misleading if thermal effects are strong.

H_c as a function of temperature for Fe nanowires with varying d_w is shown in Fig. 6. H_c as a function of T decreases the fastest for $d_w = 5.5$ nm, and the slowest for $d_w = 39$ nm. This indicates that thermal fluctuations are stronger for thinner wires. The variation of H_c with d_w at low temperatures shows exactly the opposite trend to that at room temperature. All data were fitted by Eq. (7) with $m = \frac{3}{2}$. From these fits, H_{c0} and E_{00} can be obtained. The same procedure is repeated for Co and Ni as well. H_{c0} as a function of d_w for Fe, Co, and Ni is shown in Fig. 7. Quite interestingly, it is seen that for each material, there is a critical diameter (d_c), where a transition of coercivity behavior is clearly observed. When d_w is below d_c, H_{c0} remains nearly constant; while above d_c, H_{c0} decreases monotonically with increasing d_w.

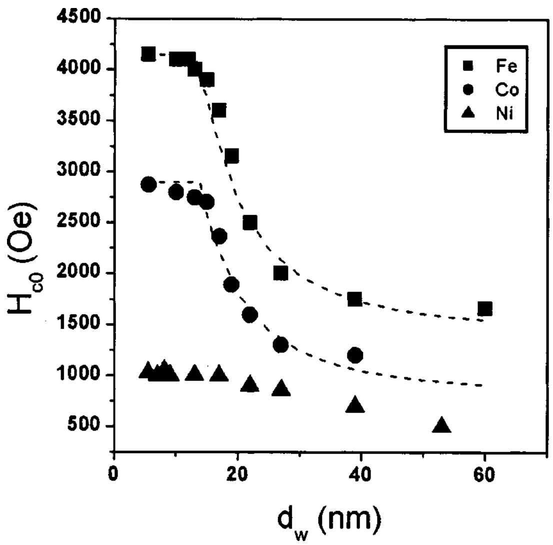

FIG. 7. Zero-temperature coercivity H_{c0} as a function of d_w for Fe and Co; the dashed lines are fits to Eqs. (9) and (10).

This behavior shows some similarity with the scenario of conventional reversal for small particles: when the diameter is smaller than a critical diameter, magnetization reversal proceeds by coherent rotation, which results in coercivity being independent of diameter; when the diameter is larger than the critical diameter, magnetization reversal takes place by curling, with coercivity decreasing with increasing diameter. The reduced coercivity for curling reversal of an infinite cylinder is

$$H_c = \frac{2\pi(2.08)^2 A}{M_s {d_w}^2}. \tag{8}$$

The critical diameters for curling reversal $2.08A^{1/2}/M_s$ (Ref. 12) are calculated to be 12, 15, and 27 nm for Fe, Co, and Ni, respectively. Following the ${d_w}^{-2}$ dependence suggested by Eq. (8), we have fitted our zero-temperature coercivity data for Fe and Co to the expression

$$H_{c0} = H_0 \quad d_w < d_c, \tag{9}$$

$$H_{c0} = H_1 + (H_0 - H_1)(d_c/d_w)^2 \quad d_w \geqslant d_c. \tag{10}$$

The fits are shown by the dashed lines in Fig. 7, and the parameters are H_0 (Fe) = 4.1, H_1 (Fe) = 1.4 kOe, and d_c (Fe) = 13.8 nm and H_0 (Co) = 2.8, H_1 (Co) = 0.8 kOe, and d_c (Co) = 14.5 nm. A fit was not attempted for Ni because d_c is in the range 20–40 nm, which cannot be determined due to insufficient data.

For Fe and Co, the agreement between the experimental and calculated d_c values is reasonably good. The zero-temperature coercivity H_{c0} for thin wires is 4.1, 2.9, and 1.0 kOe for Fe, Co, and Ni, respectively. These values are 0.37, 0.33, and 0.32, respectively, those of the shape anisotropy field for an infinite cylinder, namely, $2\pi M_s$. While the fits of Fig. 7 show an approximate ${d_w}^{-2}$ behavior similar to that predicted by the curling mode [Eq. (8)], our data are more complex presumably due to the localized reversal phenomenon. For $d_w < d_c$, the nucleation mechanism is a localized quasicoherent mode of the type discussed in Ref. 15. For $d_w > d_c$, the mode can be classified as "localized curling." This interpretation is not only supported by the present experimental results, but is also compatible with recent simulations dealing with reversal dynamics in nanowires,[23] although no rigorous treatment of reversal modes has been envisaged there.

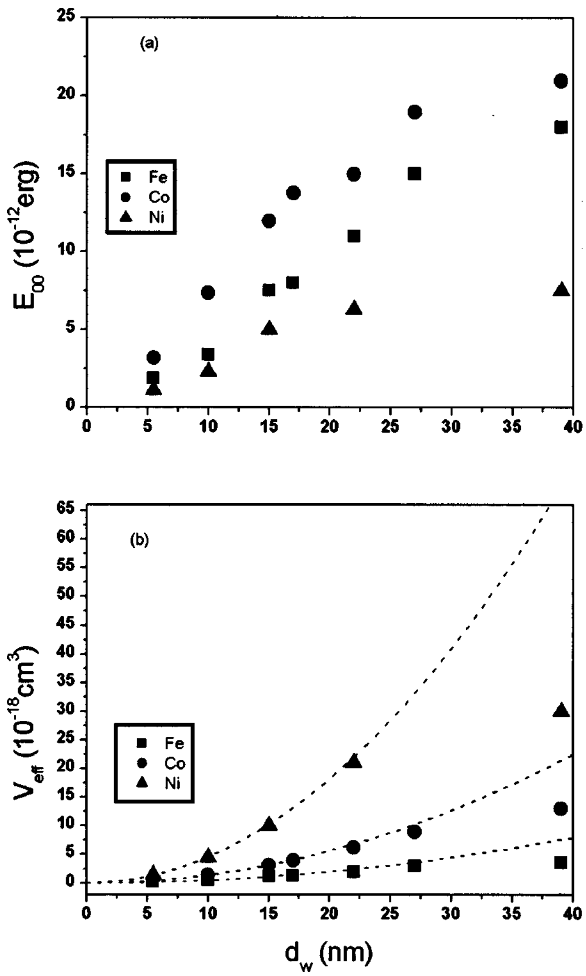

FIG. 8. (a) Zero-temperature energy barrier E_{00} and (b) effective volume of reversal $V_{\rm eff}$ as a function of d_w. The dashed lines in (b) are fitting curves.

E_{00} as a function of d_w is shown in Fig. 8(a). It is seen that E_{00} increases monotonically with increasing d_w for all three materials. The energy barrier can be approximately converted to an effective volume of magnetization reversal by using the formula[13]

$$E_{00} \equiv H_{c0} M_{s0} V_{\rm eff}. \tag{11}$$

It would be interesting to know how $V_{\rm eff}$ is related to structural and intrinsic properties. Using the E_{00}, M_{s0}, and H_{c0} obtained above, $V_{\rm eff}$ for Fe, Co, and Ni as a function of d_w is plotted in Fig. 8(b). It can be seen that $V_{\rm eff}$ increases monotonically with increasing d_w, being more rapid for larger d_w. The dashed lines are fits assuming $V_{\rm eff} \propto {d_w}^2$, that is, $V_{\rm eff}$ is proportional to the cross-sectional area of the wires. We see that these curves fit the experimental data fairly well, until the largest d_w, where the experimental $V_{\rm eff}$ is smaller than the fitting curves. This implies that $V_{\rm eff}$ is strongly dependent on lateral dimensions, while relatively independent of wire length, provided that wires are long enough. It is also seen that at identical d_w, $V_{\rm eff}$ is the largest for Ni and the smallest for Fe, which is similar to the trend of V^*. Note that the difference in the diameter dependence of V^* and $V_{\rm eff}$ lies in the fact that the relationship between V^* and $V_{\rm eff}$ depends on the energy barrier model, which is usually nonlinear.[31]

F. Physical origin of energy barriers

Until now, we have treated the quantities H_0, E_0, and m in Eq. (6) as phenomenological parameters. However, the following calculation shows that these quantities have a well-defined real-structure origin and lead to explicit predictions for effective volume of reversal and coercivities. In particular, we focus on a qualitative explanation for the experimental coercivity being often of the order of one-third of the anisotropy field (see Sec. III C).

We consider a nearly homogeneous thin nanowire, which has a small defect with slightly different anisotropy and grain misalignment. Ignoring the radial dependence of the magnetization, the free energy can be written as

$$E=\pi R^2\int\left\{A\left(\frac{\partial\phi}{\partial x}\right)^2-K(x)\cos[\phi-\theta(x)]-h\cos\phi\right\}dx, \tag{12}$$

where R is the wire radius, ϕ is the angle between magnetization and the wire axis, θ is an effective grain misalignment angle, and $h=M_sH$. We assume a small defect with $K(x)=K_s\text{-}a\Delta K\delta(x)$, where K_s is the shape anisotropy, a is the thickness of the defect, and there is a grain misalignment $\theta(x)=a\theta_0\delta(x)$. The localization length and coercivity can be obtained by minimizing the free energy, and the results are

$$H_{c0}=H_{Ks}\left(1-\frac{A}{K_sR_L{}^2}-\frac{3(2a\theta_0/R_L)^{2/3}}{4}\right), \tag{13}$$

where the anisotropy field $H_{Ks}\approx 2\pi M_s$, and $R_L=2A/(a\Delta K)$ is the localization length. The corresponding field dependence of the energy barrier is

$$E_B(H)=K_sV_0\left(1-\frac{H}{H_{c0}}\right)^{3/2}, \tag{14}$$

where $V_0=16\pi R^2R_L(2a\theta_0/R_L)^{1/3}/3^{3/2}$ represents an effective volume of magnetization reversal.

It is interesting to estimate the size of the defect that could cause the amount of reduction in H_c observed experimentally (i.e., $H_{c0}\approx H_{Ks}/3$). A coercivity reduction by a factor of $\frac{1}{3}$ is realized when the sum of the second and third terms in the parentheses of Eq. (13) is equal to $\frac{2}{3}$. Assuming an anisotropy reduction of $\Delta K=K_s/2$, where $K_s\approx\pi M_s^2$, and a grain misalignment of $\theta_0=1$ yields, for Fe, a calculated defect thickness $a\approx 5$ nm. It should be noted, however, that the exact solution of Eq. (12) is only valid for very small defects, that is, when the problem can be treated perturbatively. The present extrapolation, down to $H_{Ks}/3$, is therefore largely qualitative.

Equations (12) and (13) show how structural disorder affects the coercivity and the energy barrier of the nucleation mode, respectively, and puts the phenomenological model of the previous subsections on a sound physical basis. In particular, Eq. (13) reveals how imperfections tend to reduce the coercivity, irrespective of their physical nature. Two mechanisms are explicitly taken into account in this simple model, soft regions and misaligned grains, but future work with higher-order corrections to Eq. (13) and detailed information on defect structures are needed to make the model truly quantitative.

IV. DISCUSSION AND CONCLUSIONS

As discussed previously, magnetization reversal in thin wires starts by a localized mode having the cross-sectional symmetry of the coherent-rotation mode.[15] Since the transition from the coherent-rotation mode to the curling mode reflects the competition between exchange and magnetostatic self-interaction energies and since this competition is realized in the plane perpendicular to the wire axis,[31] we conclude that a similar transition is responsible for the observed curlinglike diameter dependence of coercivity.

Zero-temperature coercivity values for thin wires being roughly one-third of the anisotropy field indicates that the effective energy barrier is reduced significantly from the shape anisotropy of an infinite cylinder. Our model calculation indicates that the reduction is caused by wire imperfections. Such imperfections include polycrystallinity, compositional inhomogeneities, the shape of wire ends, and wire-diameter fluctuations. Experiments show that critical lengths and coercivity both scale with magnetization, suggesting that defects related to ‘‘shape’’ such as irregular wire ends and diameter fluctuations are the most important factors. Numerical simulations are underway to clarify this issue. Note, furthermore, that activation volumes determined from Eq. (2) tend to differ from those obtained using other methods by about 20% to 30%. Resolving these differences goes beyond the scope of this work and remains a challenge for future research.

The temperature dependence of coercivity shows that the field dependence of the energy barrier obeys a $\frac{3}{2}$-power law. It is shown by both our model calculation and Ref. 29 that the physical origin of the $\frac{3}{2}$-power law is the nonsymmetric energy landscape, for example, grain misalignment. The $\frac{3}{2}$-power law is actually valid for a variety of materials and reversal mechanisms, and therefore may not necessarily be associated with the Stoner-Wohlfarth model.

In conclusion, magnetic properties of ferromagnetic nanowire arrays have been investigated between room temperature and liquid-helium temperature. The temperature dependence of the coercivity yields a $\frac{3}{2}$-power law for the field dependence of the energy barriers responsible for hysteresis. This result is in agreement with general theoretical arguments and with detailed model calculations. The zero-temperature coercivity shows a sharp transition as a function of the wire diameter: below the critical diameter d_c, coercivity remains nearly constant; above d_c, it decreases with increasing d_w and is proportional to $d_w{}^{-2}$. For thin wires, H_{c0} is roughly one-third of the shape anisotropy field. Both the reduced coercivity and the observed small activation volumes are caused by wire imperfections leading to localized magnetization reversal.

ACKNOWLEDGMENTS

The authors would like to thank NRI, CMRA, and IBM for financial support.

*Present address: IBM T. J. Watson Research Center, Yorktown Heights, NY 10598. E-mail: haozeng@us.ibm.com

[1] J. L. Costa-Krämer, Phys. Rev. B **55**, R4875 (1997).
[2] C. Beeli, B. Doudin, and P. Stadelmann, Phys. Rev. Lett. **75**, 4630 (1995).
[3] K. Liu, K. Nagodawithana, P. C. Searson, and C. L. Chien, Phys. Rev. B **51**, 7381 (1995).
[4] S. Sun, C. B. Murray, D. Weller, L. Folks, and A. Moser, Science **287**, 1989 (2000).
[5] T. M. Whitney, J. S. Jiang, P. C. Searson, and C. L. Chien, Science **261**, 1318 (1993).
[6] J. Li, C. Papadopoulos, and J. M. Xu, Appl. Phys. Lett. **75**, 367 (1999).
[7] C. Chappert, H. Bernas, J. Ferré, V. Kottler, J.-P. Jamet, Y. Chen, E. Cambril, T. Devolder, F. Pousseaux, V. Mathet, and H. Launois, Science **280**, 1919 (1998) S. Y. Chou, M. S. Wei, P. R. Krauss, and P. B. Fisher, J. Appl. Phys. **76**, 6673 (1994).
[8] H. Masuda, H. Yamada, M. Satoh, and H. Asoh, Appl. Phys. Lett. **71**, 2770 (1997).
[9] S. Kawai and R. Ueda, J. Electrochem. Soc. **122**, 32 (1975) M. Shiraki, Y. Wakui, T. Tokushima, and N. Tsuya, IEEE Trans. Magn. **21**, 1465 (1985).
[10] D. AlMawlawi, N. Coombs, and M. Moskovits, J. Appl. Phys. **70**, 4421 (1991).
[11] D. J. Sellmyer, M. Zheng, and R. Skomski, J. Phys.: Condens. Matter **13**, R433 (2001).
[12] A. Aharoni, Phys. Status Solidi **16**, 1 (1966).
[13] W. Wernsdorfer, E. B. Orozco, K. Hasselbach, A. Benoit, B. Barbara, N. Demoncy, A. Loiseau, H. Pascard, and D. Mailly, Phys. Rev. Lett. **78**, 1791 (1997).
[14] S. Wirth, S. von Molnár, M. Field, and D. D. Awschalom, J. Appl. Phys. **85**, 5249 (1999).
[15] R. Skomski, H. Zeng, M. Zheng, and D. J. Sellmyer, Phys. Rev. B **62**, 3900 (2000).
[16] H. Zeng, M. Zheng, R. Skomski, D. J. Sellmyer, Y. Liu, L. Menon, and S. Bandyopadhyay, J. Appl. Phys. **87**, 4718 (2000); M. Zheng, L. Menon, H. Zeng, Y. Liu, S. Bandyopadhyay, R. D. Kirby, and D. J. Sellmyer, Phys. Rev. B **62**, 12 282 (2000).
[17] M. Zheng, R. Skomski, Y. Liu, and D. J. Sellmyer, J. Phys.: Condens. Matter **12**, L497 (2000).
[18] J.-E. Wegrowe, O. Fruchart, J.-P. Nozieres, D. Givord, F. Rousseaux, D. Decanini, and J.-Ph. Ansermet, J. Appl. Phys. **86**, 1028 (1999).
[19] K. O'Grady, P. Dova, and H. Laidler, Mater. Res. Soc. Symp. Proc. **517**, 231 (1998).
[20] J. G. Th. TeLintelo and J. C. Lodder, J. Appl. Phys. **76**, 1741 (1994).
[21] S. T. Chui and D.-C. Tian, J. Appl. Phys. **78**, 3965 (1995).
[22] M. E. Schabes, J. Magn. Magn. Mater. **95**, 249 (1991).
[23] D. Hinzke and U. Nowak, J. Magn. Magn. Mater. **221**, 365 (2000).
[24] Y. Jaccard, Ph. Guittienne, D. Kelly, J.-E. Wegrowe, and J.-Ph. Ansermet, Phys. Rev. B **62**, 1141 (2000).
[25] S. Wirth, M. Field, D. D. Awschalom, and S. von Molnár, Phys. Rev. B **57**, R14 028 (1998).
[26] N. Grobert, W. K. Hsu, Y. Q. Zhu, J. P. Hare, H. W. Kroto, D. R. M. Walton, M. Terrones, H. Terrones, Ph. Redlich, M. Rühle, R. Escudero, and F. Morales, Appl. Phys. Lett. **75**, 3363 (1999).
[27] L. Néel, Ann. Geofis. **5**, 99 (1949).
[28] W. F. Brown, Phys. Rev. **130**, 1677 (1963).
[29] R. H. Victora, Phys. Rev. Lett. **63**, 457 (1989).
[30] P. M. Paulus, F. Luis, M. Kröll, G. Schmid, and L. J. de Jongh, J. Magn. Magn. Mater. **224**, 180 (2001).
[31] R. Skomski and J. M. D. Coey, *Permanent Magnetism* (Institute of Physics, Bristol, 1999).